Study of $B_s \to \ell^+\ell^-\gamma$ decays in covariant quark model

S. Dubnička, A. Z. Dubničková, M. A. Ivanov, **

A. Liptaj, **, P. Santorelli, **, **, ** and C. T. Tran**, **

*Institute of Physics, Slovak Academy of Sciences,

Dúbravská cesta 9, 84511 Bratislava, Slovakia

**Department of Theoretical Physics, Comenius University,

Mlynská dolina F1, 84248 Bratislava, Slovakia

**Bogoliubov Laboratory of Theoretical Physics,

Joint Institute for Nuclear Research, 141980 Dubna, Russia

**Dipartimento di Fisica "E. Pancini", Università di Napoli Federico II,

Complesso Universitario di Monte S. Angelo,

Via Cintia, Edificio 6, 80126 Napoli, Italy

**Istituto Nazionale di Fisica Nucleare,

Sezione di Napoli, 80126 Napoli, Italy

Abstract

We study the rare radiative leptonic decays $B_s \to \ell^+\ell^-\gamma$ ($\ell = e, \mu, \tau$) within the Standard Model, considering both the structure-dependent amplitude and Bremsstrahlung. In the framework of the covariant confined quark model developed by us, we calculate the form factors characterizing the $B_s \to \gamma$ transition in the full kinematical region of the dilepton momentum squared and discuss their behavior. We provide the analytic formula for the differential decay distribution and give predictions for the branching fractions in both cases: with and without long-distance contributions. Finally, we compare our results with those obtained in other approaches.

PACS numbers: 13.20.He, 12.39.Ki, 14.40.Nd

Keywords: covariant quark model, bottom meson rare decay, form factor, decay distribution and rate

^{*}Electronic address: ivanovm@theor.jinr.ru

[†]Electronic address: andrej.liptaj@savba.sk

[‡]Electronic address: Pietro.Santorelli@na.infn.it

[§]Electronic address: tran@na.infn.it; corresponding author

I. INTRODUCTION

The rare radiative decays $B_q \to \ell^+\ell^-\gamma$ with $\ell = e, \mu, \tau$ and q = d, s are of great interest for several reasons. First, they are complementary to the well-known decays $B \to K^{(*)}\ell^+\ell^-$ and therefore, provide us with extra tests of the Standard Model (SM) predictions for processes which proceed at loop level. Second, this process is not helicity suppressed as compared with the pure leptonic decays $B_q \to \ell^+\ell^-$ due to the appearance of a photon in the final state. Theoretical estimates of the decay branching fractions have shown that $\mathcal{B}(B_s \to \mu^+\mu^-\gamma)$ may be an order of magnitude larger than $\mathcal{B}(B_s \to \mu^+\mu^-)$.

There is a number of theoretical calculations of the branching fractions $\mathcal{B}(B_q \to \ell^+ \ell^- \gamma)$ performed in different approaches. Among them one can mention the early studies in the framework of: a constituent quark model [1], light-cone QCD sum rules [2, 3], and the lightfront model [4]. The structure-dependent amplitude of the decays $B_s \to \ell^+\ell^-\gamma$ was analyzed in Ref. [5] by taking a universal form for the form factors, which is motivated by QCD and related to the light-cone wave function of the B_s meson. In Ref. [6] it was shown that efficient constraints on the behavior of the form factors can be obtained from the gauge-invariance requirement of the $B_q \to \ell^+\ell^-\gamma$ amplitude, as well as from the resonance structure of the form factors and their relations at large photon energies. Universality of nonperturbative QCD effects in radiative B decays was studied in Ref. [7]. In Ref. [8] long-distance QCD effects in the $B_{d/s} \to \ell^+\ell^-\gamma$ decays were analyzed. It was shown that the contribution of light vector-meson resonances related to the virtual photon emission from valence quarks of the B meson gives sizable impact on the dilepton differential distribution. In Ref. [9] the $B_{d/s} \rightarrow \gamma$ transition form factors were calculated within the relativistic dispersion approach based on the constituent quark picture. A detailed analysis of the charm-loop contributions to the radiative leptonic decays was also performed. Very recently, a novel strategy to search for the decays $B_s \to \mu^+ \mu^- \gamma$ in the event sample selected for $B_s \to \mu^+ \mu^-$ searches was presented [10].

In this paper we calculate the matrix elements and the differential decay rates of the decays $B_s \to \ell^+\ell^-\gamma$ in the framework of the covariant confined quark model previously developed by us (see, e.g., Ref. [11]). This is a quantum-field theoretical model based on relativistic Lagrangians which effectively describe the interaction of hadrons with their constituent quarks. The quark confinement is realized by cutting the integration variable,

which is called the proper time, at the upper limit. The interaction with the electromagnetic field is introduced by gauging the interaction Lagrangian in such a way to keep gauge invariance of the matrix elements at all calculation steps. This model has been successfully applied for the description of the matrix elements and form factors in the full kinematical region in semileptonic and rare decays of heavy mesons as well as baryons (see, e.g., Refs. [12–17]).

The rest of the paper is organized as follows. In Sec. II we give a necessary brief sketch of our approach. The introduction of electromagnetic interactions in the model is described in Sec. III. Sec. IV is devoted to the calculation of the decay matrix elements. We also briefly discuss their gauge invariance. In Sec. V we recalculate the formula for the twofold decay distribution in terms of the Mandelstam variables (t, s). Then we integrate out the t variable analytically and present the expression for the dilepton differential distribution. In Sec. VI we provide numerical results for the form factors, the differential decay widths, and the branching fractions. A comparison with existing results in the literature is included. Finally, we conclude in Sec. VII.

II. BRIEF SKETCH OF THE COVARIANT CONFINED QUARK MODEL

The covariant confined quark model (CCQM) has been developed by our group in a series of papers. In this section, we mention several key elements of the model only for completeness. For a more detailed description of the model, as well as the calculation techniques used for the quark-loop evaluation, we refer to Refs. [11–18] and references therein.

In the CCQM, the interaction Lagrangian of the B_s meson with its constituent quarks is constructed from the hadron field $B_s(x)$ and the interpolating quark current $J_{B_s}(x)$:

$$\mathcal{L}_{\text{int}} = g_{B_s} B_s(x) J_{B_s}(x) + H.c., \tag{1}$$

where the latter is given by

$$J_{B_s}(x) = \int dx_1 \int dx_2 \, F_{B_s}(x; x_1, x_2) \bar{b}^a(x_1) i \gamma_5 s^a(x_2). \tag{2}$$

The hadron-quark coupling g_{B_s} is obtained with the help of the compositeness condition, which requires the wave function renormalization constant of the hadron to be equal to zero $Z_H = 0$. Here, $F_{B_s}(x; x_1, x_2)$ is the vertex function whose form is chosen such as to reflect

the intuitive expectations about the relative quark-hadron positions

$$F_{B_s}(x; x_1, x_2) = \delta^{(4)} \left(x - w_1 x_1 - w_2 x_2 \right) \Phi_{B_s} \left[(x_1 - x_2)^2 \right], \tag{3}$$

where we require $w_1 + w_2 = 1$. We actually adopt the most natural choice

$$w_1 = \frac{m_b}{m_b + m_s}, \qquad w_2 = \frac{m_s}{m_b + m_s},$$
 (4)

in which the barycenter of the hadron is identified with that of the quark system. The interaction strength $\Phi_{B_s}[(x_1-x_2)^2]$ is assumed to have a Gaussian form which is, in the momentum representation, written as

$$\widetilde{\Phi}_{B_s} \left(-p^2 \right) = \exp \left(p^2 / \Lambda_{B_s}^2 \right). \tag{5}$$

Here, Λ_{B_s} is a hadron-related size parameter, regarded as an adjustable parameter of the model. Additional free parameters include the constituent quark masses and a universal cutoff parameter λ_{cutoff} related to the embedded infrared confinement of constituent quarks inside hadrons. In this paper we use the results of the updated fit performed in Refs. [16, 19, 20]. The model parameters involved in this paper are given by (in GeV)

$$\frac{m_{u/d} \quad m_s \quad m_c \quad m_b \quad \lambda \quad \Lambda_{B_s}}{0.241 \quad 0.428 \quad 1.67 \quad 5.04 \quad 0.181 \quad 2.05}.$$
 (6)

Once these parameters are fixed, one can employ the CCQM as a frame-independent tool for hadronic calculation. The parameters are determined from a least-squares fit to available experimental data and some lattice calculations. We have observed that the errors of the fitted parameters are within 10%. Besides, based on a comparison of our predictions with experimental data and lattice QCD in previous studies, we estimate the theoretical error of the CCQM to be of the order of 10%.

III. ELECTROMAGNETIC INTERACTIONS

Within the CCQM framework, interactions with electromagnetic fields are introduced as follows. First, one gauges the free-quark Lagrangian in the standard manner by using minimal substitution

$$\partial^{\mu}q_{i} \to (\partial^{\mu} - ie_{q_{i}}A^{\mu})q_{i} \tag{7}$$

that gives the quark-photon interaction Lagrangian

$$\mathcal{L}_{\text{int}}^{\text{em-min}}(x) = \sum_{q} e_q \bar{q}(x) \mathcal{A}(x) q(x). \tag{8}$$

In order to guarantee local invariance of the strong interaction Lagrangian, one multiplies each quark field $q(x_i)$ in $\mathcal{L}_{\text{int}}^{\text{str}}$ with a gauge field exponential. One then has

$$q_i(x_i) \to e^{-ie_{q_i}I(x_i,x,P)}q_i(x_i), \tag{9}$$

where

$$I(x_i, x, P) = \int_{x}^{x_i} dz_{\mu} A^{\mu}(z).$$
 (10)

The path P connects the endpoints of the path integral.

It is readily seen that the full Lagrangian is invariant under the transformations

$$q_{i}(x) \rightarrow e^{ie_{q_{i}}f(x)}q_{i}(x),$$

$$\bar{q}_{i}(x) \rightarrow \bar{q}_{i}(x)e^{-ie_{q_{i}}f(x)},$$

$$A^{\mu}(x) \rightarrow A^{\mu}(x) + \partial^{\mu}f(x).$$
(11)

One then expands the gauge exponential up to the required power of $e_q A_\mu$ needed in the perturbative series. This will give rise to a second term in the nonlocal electromagnetic interaction Lagrangian $\mathcal{L}_{\rm int}^{\rm em-nonloc}$. At first glance, it seems that the results will depend on the path P taken to connect the endpoints of the path integral in Eq. (10). However, one needs to know only the derivatives of the path integral expressions when calculating the perturbative series. Therefore, we use the formalism suggested in Refs. [21, 22], which is based on the path-independent definition of the derivative of I(x, y, P)

$$\frac{\partial}{\partial x^{\mu}}I(x,y,P) = A_{\mu}(x). \tag{12}$$

As a result of this rule, the Lagrangian describing the nonlocal interaction of the B_s meson, the quarks, and electromagnetic fields reads (to the first order in the electromagnetic charge)

$$\mathcal{L}_{\text{int}}^{\text{em-nonloc}}(x) = ig_{B_s}B_s(x) \int dx_1 \int dx_2 \int dz \left(\bar{b}(x_1)\gamma_5 s(x_2)\right) A_{\mu}(z) E^{\mu}(x; x_1, x_2, z), \quad (13)$$

$$E^{\mu}(x; x_1, x_2, z) = \int \frac{d^4p_1}{(2\pi)^4} \int \frac{d^4p_2}{(2\pi)^4} \int \frac{d^4q}{(2\pi)^4} \exp[-ip_1(x_1 - x) + ip_2(x_2 - x) + iq(z - x)]$$

$$\times \left\{ e_b(q^{\mu}w_2 - 2p^{\mu})w_2 \int_0^1 d\tau \tilde{\Phi}'_{B_s} \left[-(p - w_2q)^2\tau - p^2(1 - \tau) \right] \right\}$$

$$-e_s(q^{\mu}w_1 + 2p^{\mu})w_1 \int_0^1 d\tau \tilde{\Phi}'_{B_s} \left[-(p + w_1q)^2\tau - p^2(1 - \tau) \right] \right\}, \quad (14)$$

where $p = w_2 p_1 + w_1 p_2$.

IV. MATRIX ELEMENTS OF THE DECAYS $B_S \to \ell^+\ell^-\gamma$

The decays $B_s \to \ell^+\ell^-\gamma$ are described by three sets of diagrams shown in Figs. 1-3. Diagrams from the first set (Fig. 1) correspond to the case when the real photon is emitted from the quarks or the meson-quark vertex. The effective Hamiltonian describing the $b \to s\ell^+\ell^-$ weak transition is written as

$$\mathcal{H}_{\text{eff}}^{b \to s \ell^+ \ell^-} = \frac{G_F}{\sqrt{2}} \frac{\alpha_{\text{em}}}{2\pi} \lambda_t \Big[C_9^{\text{eff}} \left(\bar{s} \gamma^{\mu} (1 - \gamma_5) b \right) \left(\bar{\ell} \gamma_{\mu} \ell \right) - \frac{2\tilde{m}_b}{q^2} C_7^{\text{eff}} \left(\bar{s} i \sigma^{\mu\nu} q_{\nu} (1 + \gamma_5) b \right) \left(\bar{\ell} \gamma_{\mu} \ell \right) + C_{10} \left(\bar{s} \gamma^{\mu} (1 - \gamma_5) b \right) \left(\bar{\ell} \gamma_{\mu} \gamma_5 \ell \right) \Big], \tag{15}$$

where $\lambda_t = V_{tb}V_{ts}^*$, and \tilde{m}_b is the QCD quark mass which is different from the constituent quark mass m_b used in our model. Here and in the following we denote the QCD quark masses with a tilde to distinguish them from the constituent quark masses used in the model (see Eq. (6)). The Wilson coefficients $C_7^{\text{eff}} = C_7 - C_5/3 - C_6$ and C_{10} depend on the scale parameter μ . The Wilson coefficient C_9^{eff} effectively takes into account, first, the contributions from the four-quark operators \mathcal{O}_i (i = 1, ..., 6) and, second, nonperturbative effects coming from the $c\bar{c}$ -resonance contributions which are as usual parametrized by the

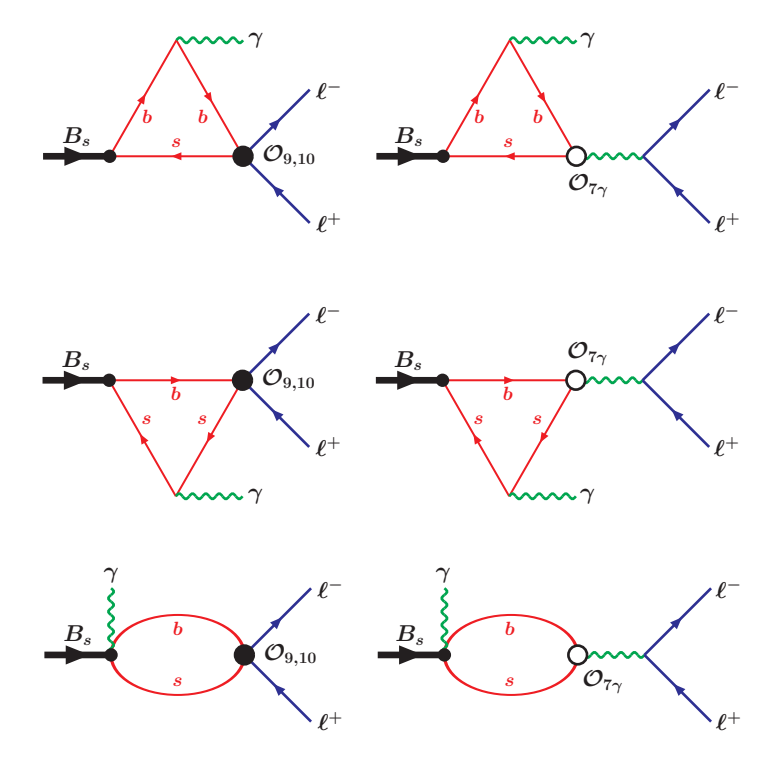


FIG. 1: Diagrams which contribute to the decays $B_s \to \ell^+ \ell^- \gamma$ with the real photon emitted from the quarks or the meson-quark vertex.

Breit-Wigner ansatz [23]:

$$C_9^{\text{eff}} = C_9 + C_0 \left\{ h(\hat{m}_c, s) + \frac{3\pi}{\alpha^2} \kappa \sum_{V_i = \psi(1s), \psi(2s)} \frac{\Gamma(V_i \to \ell^+ \ell^-) m_{V_i}}{m_{V_i}^2 - q^2 - i m_{V_i} \Gamma_{V_i}} \right\}$$

$$-\frac{1}{2} h(1, s) \left(4C_3 + 4C_4 + 3C_5 + C_6 \right)$$

$$-\frac{1}{2} h(0, s) \left(C_3 + 3C_4 \right) + \frac{2}{9} \left(3C_3 + C_4 + 3C_5 + C_6 \right),$$

$$(16)$$

where $C_0 \equiv 3C_1 + C_2 + 3C_3 + C_4 + 3C_5 + C_6$, $\hat{m}_c = \tilde{m}_c/M_{B_s}$, $s = q^2/M_{B_s}^2$, and $\kappa = 1/C_0$. Here,

$$h(\hat{m}_c, s) = -\frac{8}{9} \ln \frac{\tilde{m}_b}{\mu} - \frac{8}{9} \ln \hat{m}_c + \frac{8}{27} + \frac{4}{9} x$$

$$-\frac{2}{9} (2+x) |1-x|^{1/2} \begin{cases} \left(\ln \left| \frac{\sqrt{1-x}+1}{\sqrt{1-x}-1} \right| - i\pi \right), & \text{for } x \equiv \frac{4\hat{m}_c^2}{s} < 1, \\ 2 \arctan \frac{1}{\sqrt{x-1}}, & \text{for } x \equiv \frac{4\hat{m}_c^2}{s} > 1, \end{cases}$$

$$h(0, s) = \frac{8}{27} - \frac{8}{9} \ln \frac{\tilde{m}_b}{\mu} - \frac{4}{9} \ln s + \frac{4}{9} i\pi.$$

We will use the value of $\mu = \tilde{m}_{b\,\text{pole}}$ for the renormalization scale. The numerical values for the model-independent input parameters and the corresponding Wilson coefficients are given in Table I. The SM Wilson coefficients are taken from Ref. [24]. They were computed at the matching scale $\mu_0 = 2M_W$, and run down to the hadronic scale $\mu_b = 4.8$ GeV. The evolution of couplings and current quark masses proceeds analogously.

TABLE I: Values of the input parameters and the corresponding Wilson coefficients used in the numerical calculations [24]. Bare quark masses \tilde{m}_q are given in GeV.

\tilde{m}_c	\tilde{m}_b	$ ilde{m}_t$	$\alpha_{\rm em}(M_Z)$	$ V_{tb}V_{ts}^* $				
1.27	4.68	173.3	1/128.94	0.040				
C_1	C_2	C_3	C_4	C_5	C_6	$C_7^{ m eff}$	C_9	C_{10}
-0.2632	1.0111	-0.0055	-0.0806	0.0004	0.0009	-0.2923	4.0749	-4.3085

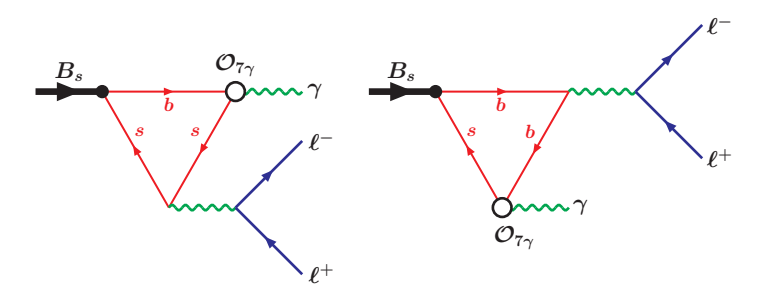


FIG. 2: Diagrams which contribute to the decays $B_s \to \ell^+\ell^-\gamma$ with the real photon emitted from the penguin.

Diagrams from the second set (Fig. 2) represent the case when the real photon is emitted from the magnetic penguin operator. The effective Hamiltonian describing the $b \to s\gamma$ electroweak transition is written as

$$\mathcal{H}_{\text{eff}}^{b \to s \gamma} = -\frac{G_F}{\sqrt{2}} \lambda_t C_7^{\text{eff}} \frac{e\tilde{m}_b}{8\pi^2} \left(\bar{s}\sigma_{\mu\nu} (1 + \gamma_5)b\right) F^{\mu\nu}. \tag{17}$$

Diagrams from the first two sets contribute to the structure-dependent (SD) part of the decay amplitude. They can be parametrized by a set of invariant form factors. In order to define the form factors, we specify our choice for the momenta in the decays as follows:

$$B_s(p_1) \to \gamma(p_2) + \ell^+(k_+) + \ell^-(k_-),$$
 (18)

where $p_1 = p_2 + k_+ + k_-$, $p_1 - p_2 = k_+ + k_- \equiv q$, with $p_1^2 = M_{B_s}^2$, $p_2^2 = 0$, $\epsilon_2^{\dagger} \cdot p_2 = 0$, and $k_+^2 = k_-^2 = m_{\ell}^2$.

We will use the definition of the $B_s \to \gamma$ transition form factors given, for instance, in Ref. [8]

$$\langle \gamma(p_2, \epsilon_2) | \bar{s} \gamma^{\mu} b | B_s(p_1) \rangle = e \epsilon_{2\alpha}^{\dagger} \varepsilon^{\mu \alpha p_1 p_2} \frac{F_V(q^2)}{M_{B_s}},$$

$$\langle \gamma(p_2, \epsilon_2) | \bar{s} \gamma^{\mu} \gamma_5 b | B_s(p_1) \rangle = i e \epsilon_{2\alpha}^{\dagger} (g^{\mu \alpha} p_1 p_2 - p_1^{\alpha} p_2^{\mu}) \frac{F_A(q^2)}{M_{B_s}},$$

$$\langle \gamma(p_2, \epsilon_2) | \bar{s} \sigma^{\mu q} b | B_s(p_1) \rangle = i e \epsilon_{2\alpha}^{\dagger} \varepsilon^{\mu \alpha p_1 p_2} F_{TV}(q^2),$$

$$\langle \gamma(p_2, \epsilon_2) | \bar{s} \sigma^{\mu q} \gamma_5 b | B_s(p_1) \rangle = e \epsilon_{2\alpha}^{\dagger} (g^{\mu \alpha} p_1 p_2 - p_1^{\alpha} p_2^{\mu}) F_{TA}(q^2). \tag{19}$$

Here we use the short notations $\sigma^{\mu q} \equiv \sigma^{\mu \beta} q_{\beta}$ and $\varepsilon^{\mu \alpha p_1 p_2} \equiv \varepsilon^{\mu \alpha \beta \delta} p_{1\beta} p_{2\delta}$.

The form factors gain contributions from the diagrams in Figs. 1 and 2 in the following manner:

$$F_{V} = M_{Bs} \left[e_{b} \tilde{F}_{V}^{b\gamma b} + e_{s} \tilde{F}_{V}^{s\gamma s} \right],$$

$$F_{A} = M_{Bs} \left[e_{b} \tilde{F}_{A}^{b\gamma b} + e_{s} \tilde{F}_{A}^{s\gamma s} + e_{b} \tilde{F}_{A}^{\text{bubble}-b} + e_{s} \tilde{F}_{A}^{\text{bubble}-s} \right],$$

$$F_{TV} = e_{b} \tilde{F}_{TV}^{b\gamma b} + e_{s} \tilde{F}_{TV}^{s\gamma s} + e_{b} \tilde{F}_{TV}^{b(\bar{\ell}\ell)b} + e_{s} \tilde{F}_{TV}^{s(\bar{\ell}\ell)s},$$

$$F_{TA} = e_{b} \tilde{F}_{TA}^{b\gamma b} + e_{s} \tilde{F}_{TA}^{s\gamma s} + e_{b} \tilde{F}_{TA}^{\text{bubble}-b} + e_{s} \tilde{F}_{TA}^{\text{bubble}-s} + e_{b} \tilde{F}_{TA}^{b(\bar{\ell}\ell)b} + e_{s} \tilde{F}_{TA}^{s(\bar{\ell}\ell)s}.$$

$$(20)$$

The process with the virtual photon emitted from the light s quark is described by the diagram in Fig. 2 (left panel). This diagram has a branch point at $q^2 = 4m_s^2$ if one does not cut the upper limit of the integration over proper time. The infrared cutoff eliminates this singularity and thereby guarantees the quark confinement. However, the physical region for q^2 in the decays $B_s \to \gamma \ell^+ \ell^-$ is extended up to $q_{\rm max}^2 = M_{B_s}^2$, which is too far from the value $q^2 = 4m_s^2$. In this case, the form factors $\tilde{F}_{TV/TA}^{s(\ell\ell)s}$ become very large and unreliable. This is a drawback of our model. We are planning to modify our approach in order to avoid such unphysical growths, and then include the intermediate ϕ resonance into this diagram. For the time being we drop the form factors $\tilde{F}_{TV/TA}^{s(\ell\ell)s}$ from the consideration.

Finally, the SD part of the amplitude is written in terms of the form factors as follows:

$$\mathcal{M}_{SD} = \frac{G_F}{\sqrt{2}} \frac{\alpha_{em} \lambda_t}{2\pi} e \epsilon_{2\alpha}^* \left\{ \left[\varepsilon^{\mu \alpha p_1 p_2} \frac{F_V(q^2)}{M_{B_s}} - i T_1^{\mu \alpha} \frac{F_A(q^2)}{M_{B_s}} \right] \left(C_9^{\text{eff}} \bar{\ell} \gamma_\mu \ell + C_{10} \bar{\ell} \gamma_\mu \gamma_5 \ell \right) \right. \\ \left. + \left[\varepsilon^{\mu \alpha p_1 p_2} F_{TV}(q^2) - i T_1^{\mu \alpha} F_{TA}(q^2) \right] \frac{2\tilde{m}_b}{a^2} C_7^{\text{eff}} \bar{\ell} \gamma_\mu \ell \right\}, \tag{21}$$

where $T_1^{\mu\alpha} \equiv (g^{\mu\alpha}p_1p_2 - p_1^{\alpha}p_2^{\mu}).$

The structure-independent part of the amplitude (Bremsstrahlung) is described by the diagrams in Fig. 3. Only the operator \mathcal{O}_{10} contributes to this process, and effectively gives

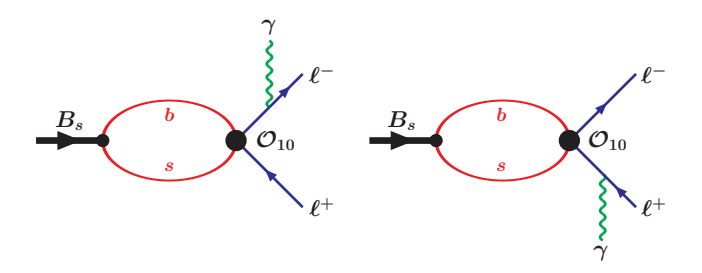


FIG. 3: Bremsstrahlung diagrams.

the leptonic decay constant f_{Bs} . One has

$$\mathcal{M}_{BR} = -i\frac{G_F}{\sqrt{2}} \frac{\alpha_{em} \lambda_t}{2\pi} e \epsilon_{2\alpha}^* (2m_\ell f_{Bs} C_{10}) \bar{u}(k_-) \left[\frac{\gamma^\alpha}{t - m_\ell^2} - \frac{\not p_1 \gamma^\alpha}{u - m_\ell^2} \right] \gamma_5 v(k_+). \tag{22}$$

Here, $t=(p_2+k_-)^2=(p_1-k_+)^2$, $u=(p_2+k_+)^2=(p_1-k_-)^2$, and $s=q^2$ so that $s+t+u=M_{B_s}^2+2m_\ell^2$. The variable t varies in the interval $t_- \leq t \leq t_+$, where the bounds t_{\pm} are given by

$$t_{\pm} = m_{\ell}^2 + \frac{1}{2}(M_{B_s}^2 - s)[1 \pm \beta(s)], \qquad \beta(s) = \sqrt{1 - \frac{4m_{\ell}^2}{s}}.$$
 (23)

One can see that $t_{\pm} = m_{\ell}^2$ at minimum recoil $s = q^2 = M_{B_s}^2$, which leads to the infrared pole in Eq. (22). A cut in the photon energy is required. In the B_s center-of-mass system one has

$$E_{\gamma} = \frac{M_{B_s}}{2} \left(1 - \frac{q^2}{M_{B_s}^2} \right) \ge E_{\gamma \, \text{min}}.$$
 (24)

Note that there are also weak annihilation diagrams with u(c) anomalous triangle in addition to the above diagrams. However, the contribution from these diagrams is much smaller than that from other diagrams as was shown in Ref. [8]. Therefore, we will drop this type of diagrams in what follows.

A few remarks should be done in respect of the calculation of the Feynman diagrams in our approach. The SD part of the matrix element is described by the diagrams in Figs. 1 and 2. These diagrams do not include ultraviolet divergences because the hadron-quark vertex functions drop off exponentially in the Euclidean region. The loop integration is performed by using the Fock-Schwinger representation for the quark propagators, and the

exponential form for the meson-quark vertex functions. The tensorial integrals are calculated by using the differential technique. The final expression for the SD part is represented as a sum of products of Lorentz structures and the corresponding invariant form factors. The form factors are described by threefold integrals in such a way that one integration is over a dimensional parameter t (proper time), which proceeds from zero to infinity, and two others are over dimensionless Schwinger parameters. The possible branch points and cuts are regularized by introducing the cutoff at the upper limit of the integration over proper time. The final integrals are calculated numerically by using the FORTRAN codes.

Then one can check that the final expression for the SD part of the amplitude is gauge invariant. Technically, it means that in addition to the gauge-invariant structures $\varepsilon^{\mu\alpha p_1p_2}$ and $T_1^{\mu\alpha} = (g^{\mu\alpha}p_1p_2 - p_1^{\alpha}p_2^{\mu})$, the amplitude has also the non-gauge-invariant pieces $g^{\mu\alpha}$ and $p_1^{\mu}p_1^{\alpha}$. We have checked numerically that the form factors corresponding to the non-gauge-invariant part vanish for arbitrary momentum transfer squared q^2 .

V. DIFFERENTIAL DECAY RATE

The twofold decay distribution is written as

$$\frac{d\Gamma}{dsdt} = \frac{1}{2^8 \pi^3 M_{B_s}^3} \sum_{\text{pol}} |\mathcal{M}|^2, \qquad \mathcal{M} = \mathcal{M}_{\text{SD}} + \mathcal{M}_{\text{BR}}, \tag{25}$$

where \sum_{pol} denotes the summation over polarizations of both the photon and leptons. The physical region was discussed in the previous section, which reads $4m_{\ell}^2 \leq s \equiv q^2 \leq M_{B_s}^2$, and $t_- \leq t \leq t_+$. It is more convenient to write the final result for the twofold decay distribution in terms of dimensionless momenta and masses:

$$\hat{X} \equiv \frac{X}{M_{B_s}^2} \quad (X = s, t, u), \quad \hat{Y} \equiv \frac{Y}{M_{B_s}} \quad (Y = m_\ell, \tilde{m}_q, f_{B_s}), \quad \text{etc.}$$
 (26)

The decay distribution is written as a sum of the structure dependent (SD) part, the Bremsstrahlung (BR), and the interference (IN) ones as follows:

$$\frac{d\Gamma}{d\hat{s}d\hat{t}} = N_t \left(\frac{d\Gamma_{\rm SD}}{d\hat{s}d\hat{t}} + \frac{d\Gamma_{\rm BR}}{d\hat{s}d\hat{t}} + \frac{d\Gamma_{\rm IN}}{d\hat{s}d\hat{t}} \right), \qquad N_t \equiv \frac{G_F^2 \alpha_{\rm em}^3 M_{B_s}^5 |\lambda_t|^2}{2^{10} \pi^4}. \tag{27}$$

One has

$$\frac{d\Gamma_{\text{SD}}}{d\hat{s}d\hat{t}} = \hat{x}^{2}B_{0} + \hat{x}(\hat{u} - \hat{t})B_{1} + (\hat{u} - \hat{t})^{2}B_{2}, \tag{28}$$

$$B_{0} = (\hat{s} + 4\hat{m}_{\ell}^{2})\Delta F - 8\hat{m}_{\ell}^{2}C_{10}^{2}(F_{V}^{2} + F_{A}^{2}), \tag{28}$$

$$B_{1} = 8\left[\hat{s}C_{10}\text{Re}(C_{9}^{\text{eff}})F_{V}F_{A} + \hat{m}_{b}C_{7}^{\text{eff}}C_{10}(F_{V}F_{TA} + F_{A}F_{TV})\right], \tag{29}$$

$$B_{2} = \hat{s}\Delta F, \tag{26}$$

$$\Delta F = (|C_{9}^{\text{eff}}|^{2} + C_{10}^{2})(F_{V}^{2} + F_{A}^{2}) + \left(\frac{2\hat{m}_{b}}{\hat{s}}\right)^{2}(C_{7}^{\text{eff}})^{2}(F_{TV}^{2} + F_{TA}^{2}) + \left(\frac{4\hat{m}_{b}}{\hat{s}}\right)C_{7}^{\text{eff}}\text{Re}(C_{9}^{\text{eff}})(F_{V}F_{TV} + F_{A}F_{TA}), \tag{29}$$

$$\frac{d\Gamma_{\text{BR}}}{d\hat{s}d\hat{t}} = (8\hat{f}_{B_{s}})^{2}\hat{m}_{\ell}^{2}C_{10}^{2}\left[\frac{1}{2}(1 + \hat{s}^{2})\hat{D}_{u}\hat{D}_{t} - (\hat{x}\hat{m}_{\ell}\hat{D}_{u}\hat{D}_{t})^{2}\right], \tag{29}$$

$$\frac{d\Gamma_{\text{IN}}}{d\hat{s}d\hat{t}} = -16\hat{f}_{B_{s}}\hat{m}_{\ell}^{2}\hat{x}^{2}\hat{D}_{u}\hat{D}_{t}\left[\frac{2\hat{x}\hat{m}_{b}}{\hat{s}}C_{10}C_{7}^{\text{eff}}F_{TV} + \hat{x}C_{10}\text{Re}(C_{9}^{\text{eff}})F_{V} + (\hat{u} - \hat{t})C_{10}^{2}F_{A}\right], \tag{30}$$

where $\hat{x} = 1 - \hat{s}$, $\hat{D}_t = 1/(\hat{t} - \hat{m}_\ell^2)$, and $\hat{D}_u = 1/(\hat{u} - \hat{m}_\ell^2)$. We have checked that all the expressions above are in agreement with those given in Ref. [9].

After integrating out the variable \hat{t} we obtain the following analytic expressions for the differential decay rate

$$\frac{d\Gamma_{\rm SD}}{d\hat{s}} = N_t \hat{x}^3 \beta \left[B_0 + \frac{1}{3} \beta^2 B_2 \right],\tag{31}$$

$$\frac{d\Gamma_{\rm BR}}{d\hat{s}} = N_t (8\hat{f}_{B_s})^2 \hat{m}_{\ell}^2 C_{10}^2 \left[\frac{1+\hat{s}^2}{\hat{x}} \ln\left(\frac{1+\beta}{1-\beta}\right) \right]$$

$$-\frac{8\hat{m}_{\ell}^2}{\hat{x}} \left(\frac{\beta}{1-\beta^2} + \frac{1}{2} \ln \left(\frac{1+\beta}{1-\beta} \right) \right) \right], \tag{32}$$

$$\frac{d\Gamma_{\rm IN}}{d\hat{s}} = -N_t 32 \hat{f}_{B_s} \hat{m}_{\ell}^2 \hat{x}^2 \ln\left(\frac{1+\beta}{1-\beta}\right) \left[C_{10} \text{Re}(C_9^{\text{eff}}) F_V + \frac{2\hat{m}_b}{\hat{s}} C_7^{\text{eff}} C_{10} F_{TV} \right], \tag{33}$$

where $\beta = \sqrt{1 - 4\hat{m}_{\ell}^2/\hat{s}}$.

VI. NUMERICAL RESULTS

In Fig. 4 we present the q^2 dependence of the calculated form factors in the full kinematical region $0 \le q^2 \le M_{B_s}^2$. The results of our numerical calculations can be approximated with high accuracy by the double-pole parametrization

$$F(q^2) = \frac{F(0)}{1 - a\hat{s} + b\hat{s}^2}, \qquad \hat{s} = \frac{q^2}{M_{B_s}^2}, \tag{34}$$

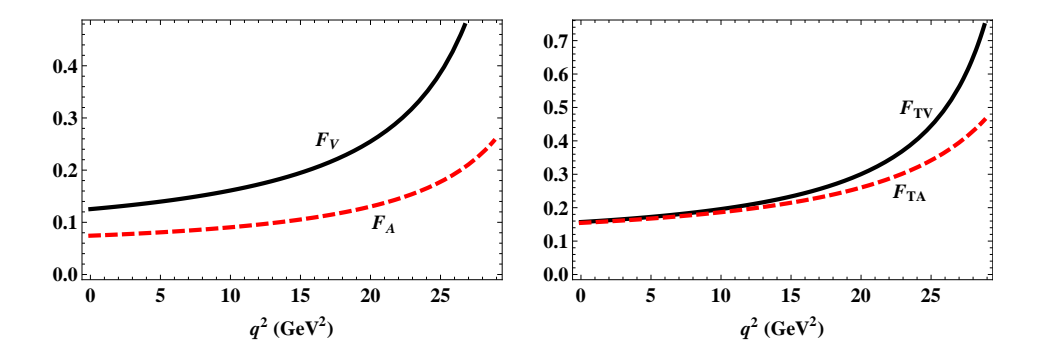


FIG. 4: Form factors for the $B_s \to \gamma$ transition.

with the relative error less than 1%. The parameters F(0), a, and b are listed in Table II. For completeness we also list here the values of the form factors at zero recoil (q_{max}^2) . As mentioned in Sec. II, the estimated theoretical error on the form factors is about 10%.

TABLE II: Parameters of the approximated $B_s \to \gamma$ form factors and their values at zero recoil.

	F_V	F_A	F_{TV}	F_{TA}
F(0)	0.13	0.074	0.16	0.15
a	0.54	0.41	0.45	0.40
b	-0.27	-0.30	-0.33	-0.26
$F(q_{\rm max}^2)$	0.69	0.26	0.76	0.47

In Figs. 5 we compare our form factors with the Kozachuk-Melikhov-Nikitin (KMN) form factors calculated in Ref. [9]. Using the definitions in Eqs. (19) and (20) we can relate our form factors $F_i(q^2)$ to the KMN form factors $F_i(q^2, 0)$ as follows (see Ref. [9] for more detail):

$$F_{V/A}(q^2, 0) = F_{V/A}(q^2), \qquad F_{TV/TA}(q^2, 0) = F_{TV/TA}(q^2) - e_b \tilde{F}_{TV/TA}^{b(\bar{l}l)b}.$$
 (35)

One can see that in the low- q^2 region ($q^2 \lesssim 20 \text{ GeV}^2$) the corresponding form factors from the two sets are very close. In the high- q^2 region, the KMN form factors steeply increase and largely exceed our form factors.

In order to have a better picture of the behavior of the form factors, in Fig. 6 we plot all of them together and compare with those from Ref. [9]. It is very interesting to note that our form factors share with the corresponding KMN ones not only similar shapes (especially

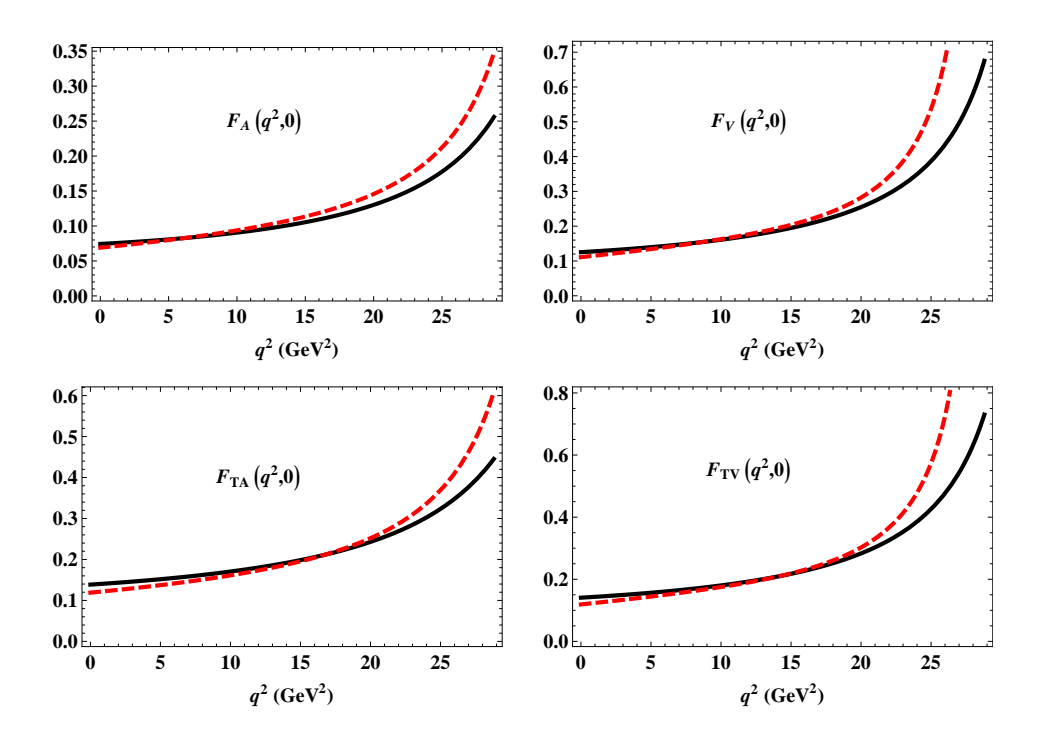


FIG. 5: Comparison of the form factors $F_i(q^2, 0)$ calculated in our model (solid lines) with those from Ref. [9] (dashed lines).

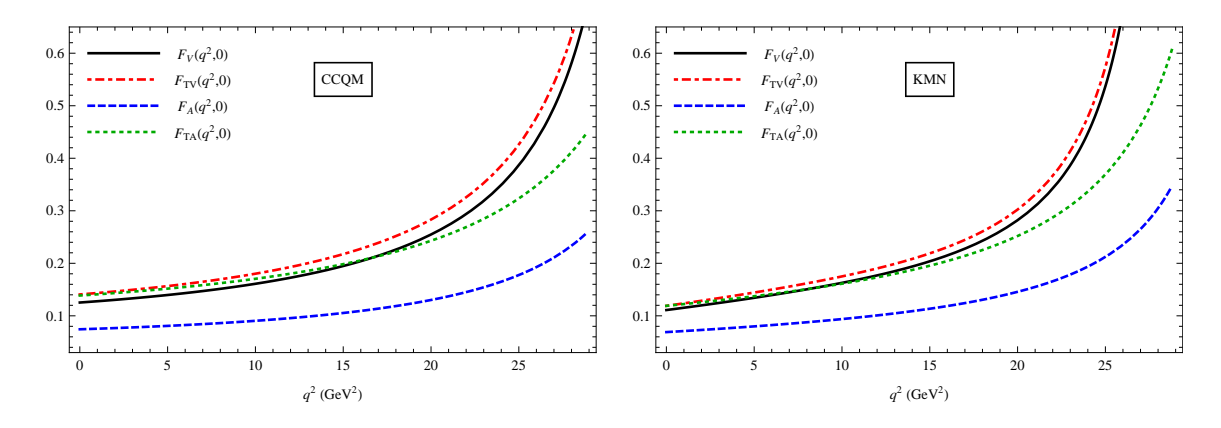


FIG. 6: Behavior of the form factors $F_i(q^2,0)$ in comparison with Ref. [9] (KMN).

in low- q^2 region) but also relative behaviors, i.e. similar relations between the form factors, in the whole q^2 region. Several comments should be made: (i) our form factors satisfy the constraint $F_{TA}(q^2,0) = F_{TV}(q^2,0)$ at $q^2 = 0$, with the common value equal to 0.135; (ii) in the small- q^2 region, $F_V(q^2,0) \approx F_{TA}(q^2,0) \approx F_{TV}(q^2,0)$; (iii) $F_V(q^2,0)$ and $F_{TV}(q^2,0)$ are approximately equal in the full kinematical range, and rise steeply in the high- q^2 region; (iv) $F_A(q^2,0)$ and $F_{TA}(q^2,0)$ are rather flat when $q^2 \to M_{B_s}^2$ as compared to $F_V(q^2,0)$ and

 $F_{TV}(q^2, 0)$. These observations show that our form factors satisfy very well the constraints on their behavior proposed by the authors of Ref. [6].

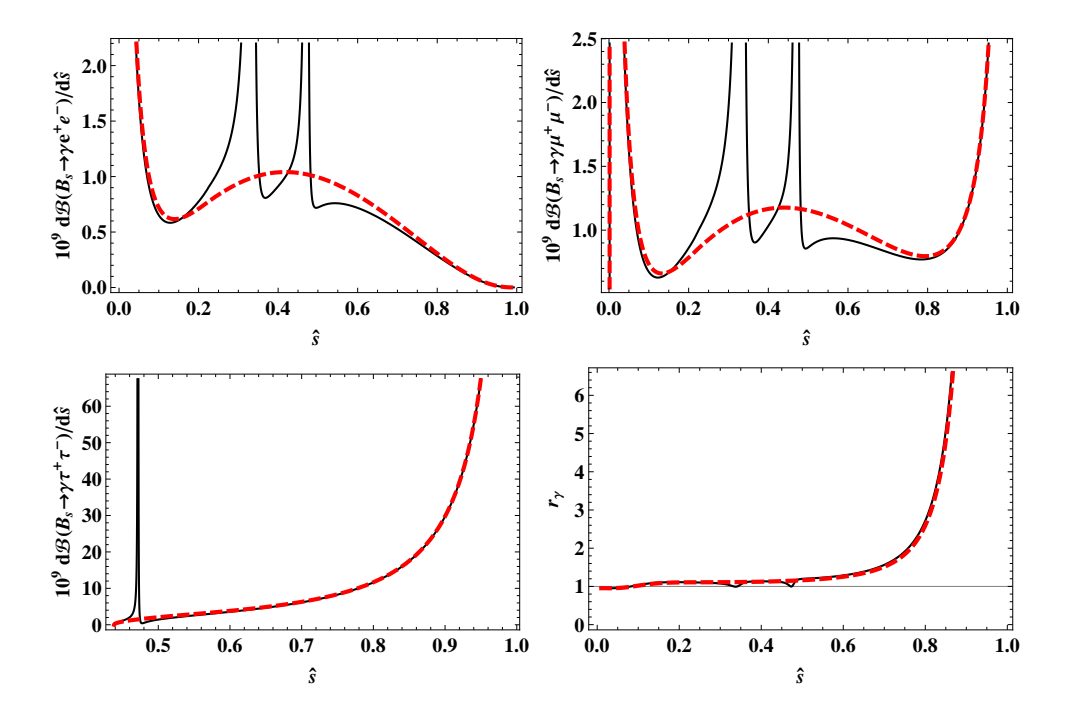


FIG. 7: Differential branching fractions $10^9 d\mathcal{B} \left(B_s \to \gamma \ell^+ \ell^-\right)/d\hat{s}$ and ratio r_γ as functions of the dimensionless variable $\hat{s} = q^2/M_1^2$ without long-distance contributions (dashed lines) and with contributions of two low lying charmonia J/ψ and $\psi(2S)$ (solid lines). The photon energy cut $E_{\gamma \min} = 20$ MeV is used.

In Fig. 7 we plot the differential branching fractions $10^9 d\mathcal{B} (B_s \to \gamma \ell^+ \ell^-)/d\hat{s}$ as functions of the dimensionless variable $\hat{s} = q^2/M_1^2$. We also plot here the ratio

$$r_{\gamma}(\hat{s}) \equiv \frac{d\mathcal{B}(B_s \to \gamma \mu^+ \mu^-)/d\hat{s}}{d\mathcal{B}(B_s \to \gamma e^+ e^-)/d\hat{s}},\tag{36}$$

which is a promising observable for testing lepton flavor universality (LFU) in these channels [25]. The ratio r_{γ} is very close to unity in low- q^2 region but far above unity at large q^2 due to Bremsstrahlung. As was pointed out in Ref. [9], in the high- q^2 region ($q^2 \gtrsim 15 \text{ GeV}^2$), the ratio r_{γ} is mainly described by the form factors $F_A(q^2)$ and $F_V(q^2)$. Therefore, knowledge of their behavior at large q^2 plays an important role in testing LFU. In Fig. 8 we plot the ratio r_{γ} at large q^2 in comparison with Ref. [9]. The ratios are very close in the range $16 \lesssim q^2 \lesssim 20 \text{ GeV}^2$ (i.e. $0.55 \lesssim \hat{s} \lesssim 0.69$), which is a result of the similarity between the form factors discussed above.

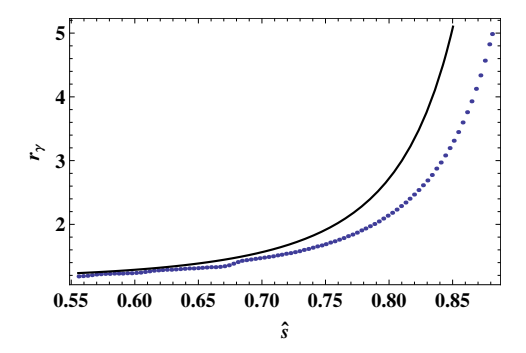


FIG. 8: Ratio $r_{\gamma}(\hat{s})$ at large \hat{s} obtained in our model (solid line) and from Ref. [9] (dotted line).

The authors of Ref. [25] suggested a useful observable

$$R_{\gamma}(\hat{s}_{1}, \hat{s}_{2}) \equiv \frac{\int_{\hat{s}_{1}}^{\hat{s}_{2}} d\hat{s} \, d\mathcal{B}(B_{s} \to \gamma \mu^{+} \mu^{-}) / d\hat{s}}{\int_{\hat{s}_{1}}^{\hat{s}_{2}} d\hat{s} \, d\mathcal{B}(B_{s} \to \gamma e^{+} e^{-}) / d\hat{s}}, \tag{37}$$

with the optimal choice $\hat{s}_1 = 0.55$ and $\hat{s}_2 = 0.8$ (corresponding to $q_1^2 = 15.8$ GeV² and $q_2^2 = 23.0$ GeV², respectively). In this range, the ratio is dominated by the form factors $F_A(q^2)$ and $F_V(q^2)$. We provide our prediction for this ratio $R_{\gamma}(0.55, 0.8) = 1.46$, about 20% larger than the prediction $R_{\gamma}(0.55, 0.8) = 1.115 \pm 0.030$ given in Ref. [25]. Note that from the results of Ref. [9], one obtains $R_{\gamma}(0.55, 0.8) = 1.32$.

In Table III we give the values of the branching fractions calculated without and with long distance contributions. In the calculation with long distance contributions, the region of two low lying charmonia is excluded by assuming $0.33 \le \hat{s} \le 0.55$, as usually done in experimental data analysis. It is seen that the Bremsstrahlung contribution to the electron mode is negligible, while for the tau mode it becomes the main part.

TABLE III: Branching fractions with (in brackets) and without long-distance contributions. The used minimal photon energy is $E_{\gamma \min} = 20$ MeV.

Si	D	BR	IN	sum
$10^9 \mathcal{B}(B_s \to \gamma e^+ e^-) \ 2.81 \ ($	2.74)	$3.0\cdot10^{-5}$	$-4.40(-4.37) \cdot 10^{-6}$	2.8 (2.7)
$10^9 \mathcal{B}(B_s \to \gamma \mu^+ \mu^-) \ 1.07 \ ($	1.00)	0.50	$-6.8(-12.9)\cdot 10^{-3}$	1.6 (1.5)
$10^9 \mathcal{B}(B_s \to \gamma \tau^+ \tau^-) \ 0.09 \ ($	0.06)	12.3	0.28 (0.18)	12.7(12.6)

Finally, in Table IV we compare our results for the branching fractions with those obtained in other approaches. In most cases, our predictions for the light leptons are smaller than those from other studies. This is due mainly to the fact that in this paper we drop the contribution from the diagram with the virtual photon emited from the s quark, which should has a sizable impact on the final results. In the case of the tau mode, the contribution from Bremsstrahlung dominates the decay branching fractions and the SD amplitude becomes less important. As a result, our prediction for $\mathcal{B}(B_s \to \gamma \tau^+ \tau^-)$ agrees well with other studies.

TABLE IV: Comparison of the branching fractions $10^9 \mathcal{B}(B_s \to \gamma \ell^+ \ell^-)$ ($\ell = e, \mu, \tau$) with other approaches. The used minimal photon energy is $E_{\gamma \min} = 20$ MeV.

Ref.	electron	muon	tau
This work	2.7	1.5	12.6
[1]	6.2	4.6	_
[2]	2.35	1.9	_
[3]	_	_	15.2
[4]	7.1	8.3	15.7
[5]	20.0	12.0	_
[8]	24.6	18.9	11.6
[26]	18.4	11.6	_
[27]	17.4	17.4	_

VII. SUMMARY AND CONCLUSIONS

We have studied the rare radiative leptonic decays $B_s \to \gamma \ell^+ \ell^-$ ($\ell = e, \mu, \tau$) in the framework of the covariant confined quark model. The relevant transition form factors have been obtained in the full kinematical range of dilepton momentum transfer squared. We found a very good agreement between our form factors and those from Ref. [9], especially in the region $q^2 \lesssim 20 \text{ GeV}^2$. We have provided predictions for the decay branching fractions and their ratio. The branching fractions for the light leptons are lower than most existing values in the literature. In our opinion, the main reason is that we have not considered the

contribution from the diagram with the virtual photon emitted from the light s quark of the B_s meson, due to the involved unphysical growths. However, we note that this diagram has no effects on the form factors $F_V(q^2)$ and $F_A(q^2)$ calculated in the present study. Therefore, the two form factors may be useful to study LFU in these rare channels, especially in the high- q^2 region. In our future works, we plan to modify our approach to treat this problem and include the diagram contribution into the process.

Acknowledgments

The work was partly supported by Slovak Grant Agency for Sciences VEGA, Grant No. 1/0158/13 and Slovak Research and Development Agency APVV, Grant No. APVV-0463-12 (S. D., A. Z. D., A. L.). S. D., A. Z. D., M. A. I, and A. L. acknowledge the support from the Joint Research Project of Institute of Physics, SAS and Bogoliubov Laboratory of Theoretical Physics, JINR, No. 01-3-1114. P. S. acknowledges the support from Istituto Nazionale di Fisica Nucleare, I.S. QFT_HEP. C. T. T. thanks Dmitri Melikhov for useful discussions.

^[1] G. Eilam, C. D. Lu, and D. X. Zhang, Phys. Lett. B **391**, 461 (1997) [hep-ph/9606444].

^[2] T. M. Aliev, A. Ozpineci, and M. Savci, Phys. Rev. D 55, 7059 (1997) [hep-ph/9611393].

^[3] T. M. Aliev, N. K. Pak, and M. Savci, Phys. Lett. B **424**, 175 (1998) [hep-ph/9710304].

^[4] C. Q. Geng, C. C. Lih, and W. M. Zhang, Phys. Rev. D **62**, 074017 (2000) [hep-ph/0007252].

^[5] Y. Dincer and L. M. Sehgal, Phys. Lett. B **521**, 7 (2001) [hep-ph/0108144].

^[6] F. Krüger and D. Melikhov, Phys. Rev. D 67, 034002 (2003) [hep-ph/0208256].

^[7] S. Descotes-Genon and C. T. Sachrajda, Phys. Lett. B 557, 213 (2003) [hep-ph/0212162].

^[8] D. Melikhov and N. Nikitin, Phys. Rev. D 70, 114028 (2004) [hep-ph/0410146].

^[9] A. Kozachuk, D. Melikhov, and N. Nikitin, Phys. Rev. D 97, 053007 (2018) [arXiv:1712.07926].

^[10] F. Dettori, D. Guadagnoli, and M. Reboud, Phys. Lett. B 768, 163 (2017) [arXiv:1610.00629].

^[11] T. Branz, A. Faessler, T. Gutsche, M. A. Ivanov, J. G. Körner, and V. E. Lyubovitskij, Phys. Rev. D 81, 034010 (2010) [arXiv:0912.3710].

^[12] M. A. Ivanov, J. G. Körner, S. G. Kovalenko, P. Santorelli, and G. G. Saidullaeva, Phys. Rev.

- D 85, 034004 (2012) [arXiv:1112.3536].
- [13] M. A. Ivanov, J. G. Körner, and C. T. Tran, Phys. Rev. D 94, 094028 (2016) [arXiv:1607.02932].
- [14] A. Faessler, T. Gutsche, M. A. Ivanov, J. G. Körner, and V. E. Lyubovitskij, Eur. Phys. J. direct C 4, 18 (2002) [hep-ph/0205287].
- [15] S. Dubnička, A. Z. Dubničková, N. Habyl, M. A. Ivanov, A. Liptaj, and G. S. Nurbakova, Few-Body Syst. 57, 121 (2016) [arXiv:1511.04887].
- [16] T. Gutsche, M. A. Ivanov, J. G. Körner, V. E. Lyubovitskij, P. Santorelli, and N. Habyl, Phys. Rev. D 91, 074001 (2015); 91, 119907(E) (2015) [arXiv:1502.04864].
- [17] T. Gutsche, M. A. Ivanov, J. G. Körner, V. E. Lyubovitskij, and P. Santorelli, Phys. Rev. D 87, 074031 (2013) [arXiv:1301.3737].
- [18] M. A. Ivanov and C. T. Tran, Phys. Rev. D **92**, 074030 (2015) [arXiv:1701.07377].
- [19] G. Ganbold, T. Gutsche, M. A. Ivanov, and V. E. Lyubovitskij, J. Phys. G 42, 075002 (2015) [arXiv:1410.3741].
- [20] A. Issadykov, M. A. Ivanov, and S. K. Sakhiyev, Phys. Rev. D 91, 074007 (2015), [arXiv:1502.05280].
- [21] S. Mandelstam, Ann. Phys. (Paris) 19, 1 (1962).
- [22] J. Terning, Phys. Rev. D 44, 887 (1991).
- [23] A. Ali, T. Mannel, and T. Morozumi, Phys. Lett. B 273, 505 (1991).
- [24] S. Descotes-Genon, T. Hurth, J. Matias, and J. Virto, J. High Energy Phys. 05, (2013) 137 [arXiv:1303.5794].
- [25] D. Guadagnoli, M. Reboud, and R. Zwicky, J. High Energy Phys. 11, (2017) 184 [arXiv:1708.02649 [hep-ph]].
- [26] D. Melikhov, A. Kozachuk, and N. Nikitin, Proc. Sci., EPS-HEP2017 (2017) 228, [arXiv:1710.02719].
- [27] W. Y. Wang, Z. H. Xiong, and S. H. Zhou, Chin. Phys. Lett. **30**, 111202 (2013) [arXiv:1303.0660].